Report

Current Biology

Rho and F-actin self-organize within an artificial cell cortex

Highlights

- An artificial cell cortex self-organizes dynamic patterns of active Rho and F-actin
- Reconstituted cortical dynamics include excitable waves and coherent oscillations
- Supported lipid bilayer fluidity is needed for traveling excitable waves
- Reconstituted dynamics require Rho activity and F-actin polymerization

Authors

Jennifer Landino, Marcin Leda, Ani Michaud, ..., Anthony G. Vecchiarelli, Andrew B. Goryachev, Ann L. Miller

Correspondence

annlm@umich.edu (A.L.M.), landinoj@umich.edu (J.L.)

In brief

In this report, Landino et al. reconstitute two types of cortical Rho and F-actin dynamics—excitable waves and coherent oscillations—on supported lipid bilayers (SLBs) using *Xenopus* egg extract. They determine that excitable waves depend on fluidity of the SLB and that waves and oscillations require Rho activity and F-actin polymerization.

Landino et al., 2021, Current Biology *31*, 5613–5621
December 20, 2021
https://doi.org/10.1016/j.cub.2021.10.021

CellPress

Current Biology

CellPress

Report

Rho and F-actin self-organize within an artificial cell cortex

Jennifer Landino,[1,*] Marcin Leda,[2] Ani Michaud,[3,4] Zachary T. Swider,[3,4] Mariah Prom,[4,7] Christine M. Field,[5] William M. Bement,[3,4,6] Anthony G. Vecchiarelli,[1] Andrew B. Goryachev,[2] and Ann L. Miller[1,8,*]

[1]Department of Molecular, Cellular, and Developmental Biology, University of Michigan, Ann Arbor, MI, USA
[2]Centre for Synthetic and Systems Biology, University of Edinburgh, Edinburgh, UK
[3]Cellular and Molecular Biology Graduate Program, University of Wisconsin-Madison, Madison, WI, USA
[4]Center for Quantitative Cell Imaging, University of Wisconsin-Madison, Madison, WI, USA
[5]Department of Systems Biology, Harvard Medical School, Boston, MA, USA
[6]Department of Integrative Biology, University of Wisconsin-Madison, Madison, WI, USA
[7]Present address: Department of Pathology and Neuroscience Research Center, Medical College of Wisconsin, Milwaukee, WI, USA
[8]Lead contact
*Correspondence: annlm@umich.edu (A.L.M.), landinoj@umich.edu (J.L.)
https://doi.org/10.1016/j.cub.2021.10.021

SUMMARY

The cell cortex, comprised of the plasma membrane and underlying cytoskeleton, undergoes dynamic reorganizations during a variety of essential biological processes including cell adhesion, cell migration, and cell division.[1,2] During cell division and cell locomotion, for example, waves of filamentous-actin (F-actin) assembly and disassembly develop in the cell cortex in a process termed "cortical excitability."[3–7] In developing frog and starfish embryos, cortical excitability is generated through coupled positive and negative feedback, with rapid activation of Rho-mediated F-actin assembly followed in space and time by F-actin-dependent inhibition of Rho.[7,8] These feedback loops are proposed to serve as a mechanism for amplification of active Rho signaling at the cell equator to support furrowing during cytokinesis while also maintaining flexibility for rapid error correction in response to movement of the mitotic spindle during chromosome segregation.[9] In this paper, we develop an artificial cortex based on *Xenopus* egg extract and supported lipid bilayers (SLBs), to investigate cortical Rho and F-actin dynamics.[10] This reconstituted system spontaneously develops two distinct types of self-organized cortical dynamics: singular excitable Rho and F-actin waves, and non-traveling oscillatory Rho and F-actin patches. Both types of dynamic patterns have properties and dependencies similar to the excitable dynamics previously characterized *in vivo*.[7] These findings directly support the long-standing speculation that the cell cortex is a self-organizing structure and present a novel approach for investigating mechanisms of Rho-GTPase-mediated cortical dynamics.

RESULTS AND DISCUSSION

Reconstituted cortex generates excitable waves of active Rho and F-actin

A cell-free system comprised of *Xenopus* egg extract containing intact actin and artificial centrosomes has previously been shown to reconstitute cortical cytokinetic patterning.[10] Microtubule-dependent signaling localizes active Rho zones at microtubule overlaps within an artificial cell cortex formed atop supported lipid bilayers (SLBs).[10] Here we endeavor to reconstitute self-organized cortical Rho patterning, independent of exogenous signals. Specifically, we adapted a similar cell-free system to investigate active Rho and filamentous actin (F-actin), waves that have previously only been observed in live cells.[7] To visualize cortical active Rho and actin dynamics, we added *Xenopus* egg extract containing recombinant probes for active Rho (Rho binding domain of Rhotekin [rGBD]) and F-actin (Utrophin calponin homology domain [UtrCH]) to SLBs designed to mimic the inner leaflet of the animal cell membrane.[10–12] We imaged active Rho and F-actin associated with SLBs using total internal reflection fluorescence (TIRF) microscopy (Figures 1A and 1B). Using this approach, we identified two distinct types of self-organized cortical dynamics: an excitable, propagating wave of active Rho and F-actin polymerization (Figure 1) and coherent, oscillatory dynamics of active Rho and F-actin (Figure 2).

Immediately after adding *Xenopus* extract to the SLB, we observed the rapid self-organization of active Rho and F-actin patterning in the form of a dramatic propagation of a solitary excitable wave (Figure 1C; Figure S1B). This remarkable phenomenon manifested as a sudden large-amplitude increase in Rho activity as discrete maxima (Figure 1C, white arrows) that rapidly spread and transformed into irregular circular waves that annihilated upon collision with each other (Figure 1C, yellow arrowheads; Video S1). Two-color imaging with high temporal resolution demonstrated that the Rho activity wave is closely followed by the actin polymerization wave (Figure 1D). This excitable behavior started and ended within 140 ± 38 s (mean ± SD, n = 5 experiments) after adding *Xenopus* egg extract to the

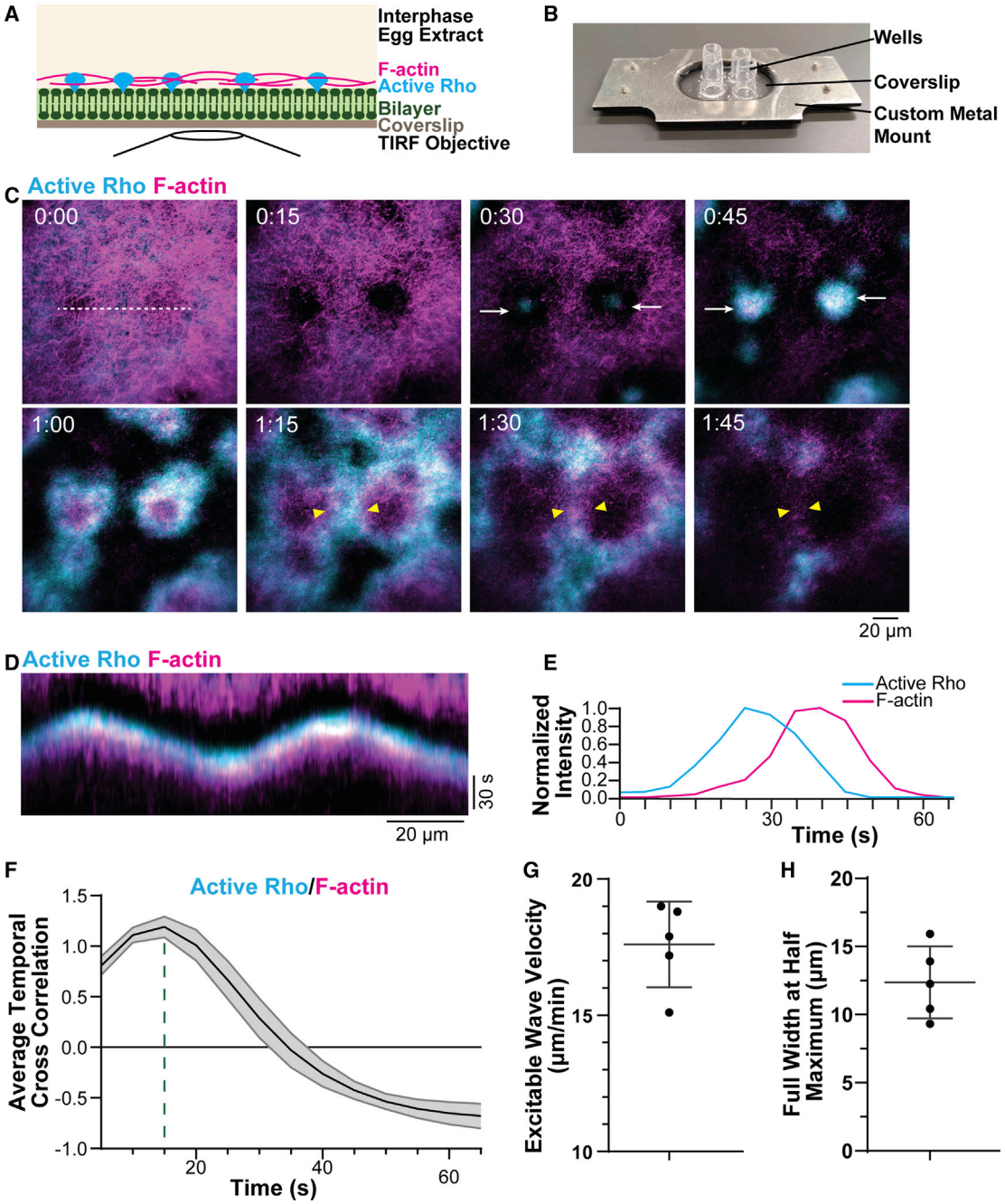

Figure 1. An artificial cortex supports the self-organization of excitable waves of active Rho and F-actin

(A) Schematic of cell-free reconstitution of cortical dynamics. Interphase *Xenopus* egg extract was added to a supported lipid bilayer atop a glass coverslip and imaged using TIRF microscopy. Active Rho (cyan) and F-actin (magenta) associated with the bilayer were visualized using recombinant GFP-tagged active Rho probe (rGBD) and Alexa Fluor 647-labeled calponin homology domain of utrophin (UtrCH).

(B) Image of the custom aluminum coverslip holder with wells attached.

(C) Micrographs (30 s difference subtraction) of traveling excitable waves of active Rho (cyan) and F-actin (magenta) that originate from discrete maxima (white arrows). Yellow arrowheads indicate wave fronts that annihilate on collision. Time is in minutes:seconds. Dashed line represents region used to generate kymograph.

(D) Kymograph of excitable waves of active Rho (cyan) and F-actin (magenta) generated from a 10-pixel-wide line shown in (C).

(E) Normalized time series of intensities of active Rho and F-actin spatially averaged over a representative 20 × 20-pixel box selected from the field of view (see Figure S1A). Moving time average of three frames.

(F) Temporal cross correlation between active Rho and F-actin intensities. Dashed line indicates the peak time shift of 15 s.

(legend continued on next page)

SLB, occurring just once per reconstituted cortex image acquisition sequence. Thus, the self-organized excitable wave observed in the reconstituted system was solitary. While the nature of wave initiation remains unclear, we observe that excitable waves propagate from well-defined active Rho foci centered in a local clearing of F-actin, suggesting that stochastic fluctuations in protein concentrations may initiate excitable wave formation.

To specifically visualize and quantify wave dynamics, we used temporal difference subtraction to computationally remove static active Rho and F-actin signal (Figure S1A).[7] We then divided the field of view into a grid of 20 × 20 pixel boxes and plotted the box-averaged and normalized fluorescence intensity of active Rho and F-actin in an individual box over time (Figure 1E). This enabled us to measure the cross-correlation between the dynamics of active Rho and F-actin within a video (Figure 1F; Figure S1C). Across multiple experiments, the time shift between the maxima of Rho activity and F-actin polymerization within excitable waves was 22.6 ± 6.3 s (mean ± SD, n = 5 experiments, 3,027 boxes, Figure S1D), which is within the same order of magnitude as the shift observed *in vivo* (48 s, Figure S1F).[7] Using kymographs to track the position and amplitude of the wave front over time, we quantified the velocity and width of the excitable waves. Excitable active Rho waves traveled at 17.6 ± 1.6 μm/minute (mean ± SD, n = 5 experiments, 151 wave fronts, Figure 1G; Figure S1E), which is similar to the velocity of cortical waves in *Xenopus* blastomeres (10.8 μm/minute, Figure S1F).[7] The full width at half maximum of the waves was 12.4 ± 2.6 μm (mean ± SD, n = 5 experiments, 678 wave fronts, Figure 1H). Taken together, our results demonstrate that solitary self-organized excitable waves of active Rho and F-actin can be generated using an artificial cell cortex system.

Active Rho and F-actin coherently oscillate in a cell-free reconstituted system

In addition to excitable waves, the reconstituted cortex self-organized into oscillatory, coherent pulses of active Rho and F-actin, which generally occurred after the appearance of an excitable wave, manifesting 13 ± 9 min (mean ± SD, n = 8 experiments) after the extract is added to the SLB. These oscillations exhibit a defined temporal period but do not result in spatially propagating waves, instead forming discrete patches on the SLB (Figures 2A, 2B, and 2C; Video S2). Alongside the appearance of oscillatory active Rho and F-actin dynamics, we also observed prominent static fluorescence signals for active Rho and F-actin that progressively accumulate on the bilayer (Figures S2A and S2B). These static signals partially mask the oscillatory dynamics of active Rho and F-actin on the SLB (Figure S2C), so we again used temporal difference subtraction (Figure S1A)[7] to computationally remove static signals prior to quantifying oscillatory dynamics.

The temporal dynamics of oscillatory active Rho and F-actin were analyzed using Morlet wavelet transform that was applied to the respective fluorescence signals spatially averaged over individual boxes (Figure 2D).[7,13] This local analysis revealed complex, spatially and temporally heterogeneous behavior with short oscillatory stretches of varying period appearing and vanishing throughout the experiment. Remarkably, spatial averaging of local Morlet spectra revealed a robust dominant oscillatory pattern with a reproducible period (Figure 2E). Across multiple experiments, we determined the period of active Rho oscillations to be 131 ± 8.6 s (mean ± SD, n = 8 experiments, 2,453 boxes, Figure S2D). This is comparable to the period of waves of active Rho previously characterized in developing *Xenopus* embryos (80–120 s, Figure S1F).[7] Using temporal cross-correlation analysis (Figure 2F; Figure S2E), we determined that oscillatory F-actin peaked on average 22.5 ± 4.1 s (mean ± SD, n = 8 experiments, 5,494 boxes) after the respective maxima of active Rho (Figure S2F), which is well matched to the time shift for excitable waves of active Rho and F-actin (Figure S1F).

Our analysis of both excitable and oscillatory active Rho and F-actin patterns demonstrates that the artificial cortex successfully reconstitutes cortical dynamics with characteristics similar to those described *in vivo* (Figure S1F).[7] Moreover, the emergence of cortical patterns, in the form of Rho and F-actin waves and oscillations, in this cell-free system reveals that the artificial cortex can self-organize independently of exogenous signaling from sources such as the nucleus or centrosomes, which are not present in our experiments.

Supported lipid bilayer fluidity enables excitable waves

We next sought to understand why excitable waves occur only once in our reconstituted system. We hypothesized that *Xenopus* egg extract contains proteins that can modify the chemical and physical properties of the SLB, so we investigated whether the presence of a "fresh" SLB was important for the formation of an excitable wave. To test this idea, we asked whether extract that produces an excitable wave can produce a second excitable wave upon transfer to a fresh SLB (Figure 3A). Indeed, another excitable wave was observed upon transfer of the same interphase egg extract to a fresh SLB (Figures 3B and 3C; Video S3), suggesting that the SLB is modified after the first excitable wave in such a way that it prevents propagation of a second excitable wave.

We next tested whether SLB fluidity was altered after the addition of *Xenopus* extract by co-imaging Cy5-labeled phosphatidylcholine (PC) alongside active Rho and F-actin oscillations. No discernable change in Cy5-PC dynamics was observed during the course of imaging (Figure 3D). We also analyzed the fluorescence recovery after photobleaching (FRAP) of Cy5-PC in the SLB before extract addition and 30 min after extract addition (Figure 3E). Before extract addition, the mobile fraction was 76.85 ± 0.82%, and the $t_{1/2}$ was 33.21 ± 2.08 s (mean ± SD, n = 6 bleach regions from two independent experiments). When Cy5-PC was bleached after the addition of extract, the fluorescence continued to slowly recover—even at times 10-fold longer than the $t_{1/2}$ of the untreated bilayer, suggesting

(G) Excitable wave velocity, 17.6 ± 1.6 μm/minute (mean ± SD), was measured over 50–60 s for 151 wave fronts across five experiments. Each dot represents the average velocity for one experiment.
(H) Full width at half maximum, 12.4 ± 2.6 μm (mean ± SD), was measured for 678 wave fronts across five experiments. Each dot represents the average full width at half maximum for one experiment.
See also Figure S1 and Video S1.

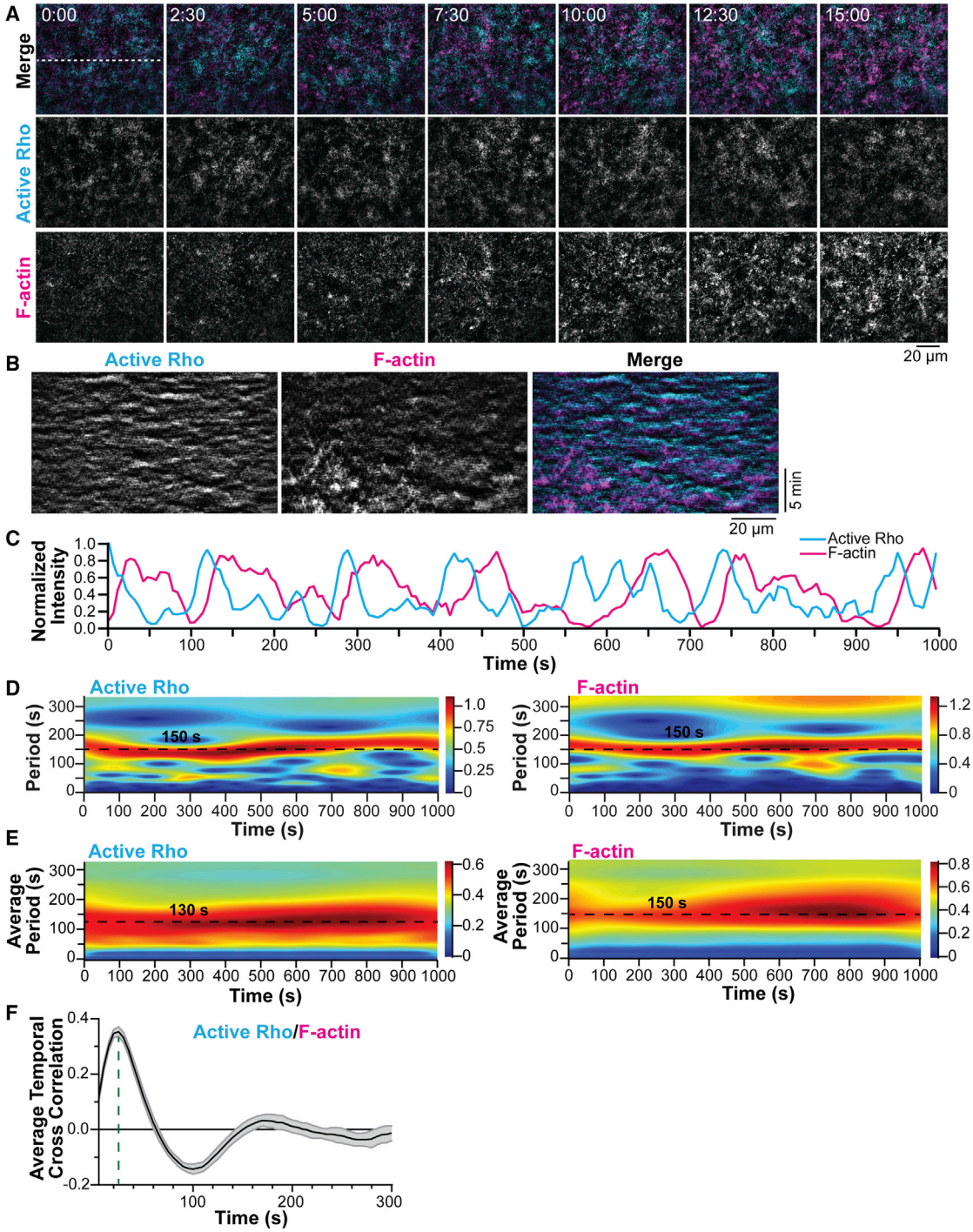

Figure 2. Active Rho and F-actin coherently oscillate within an artificial cortex

(A) Reconstituted oscillatory dynamics of active Rho (cyan) and F-actin (magenta). Time is indicated in minutes:seconds. Dashed line represents the region used to generate kymographs.

(B) Kymographs of oscillatory dynamics of active Rho (cyan) and F-actin (magenta) generated from a 10-pixel-wide line shown in (A).

(C) Normalized time series of intensities of active Rho and F-actin spatially averaged over a representative 20 × 20-pixel box selected from the field of view (see Figure S1A). Moving time average of three frames.

(D) Morlet power spectra showing the time-dependent periodicity of the active Rho and F-actin dynamics computed for the same 20 × 20-pixel box as shown in (C). Dashed lines indicate dominant oscillatory periods.

(legend continued on next page)

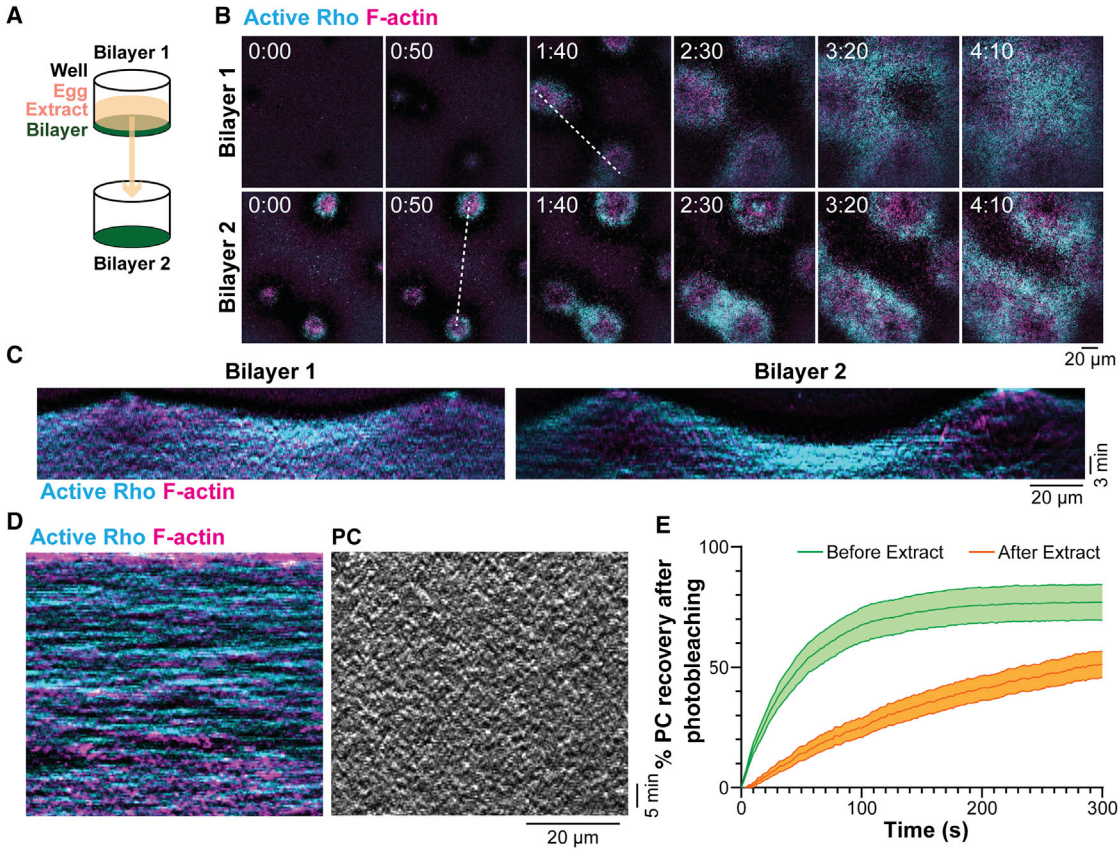

Figure 3. Supported lipid bilayer fluidity enables excitable waves

(A) Schematic of SLB transfer experiment. Interphase egg extract containing probes for active Rho and F-actin was added to a well with a fresh SLB, and an excitable wave was imaged to completion. The same extract was then transferred to a new SLB to determine if it could produce a second excitable wave.

(B) Interphase egg extract can produce a second excitable wave after transfer to a new SLB. Active Rho (cyan) and F-actin (magenta). Time is indicated in minutes:seconds. Dashed lines represent the regions used to generate kymographs.

(C) Kymographs of excitable waves of active Rho (cyan) and F-actin (magenta) generated in the same extract on two different SLBs.

(D) Kymographs of active Rho, F-actin, and phosphatidylcholine (PC) co-imaged after addition to a SLB.

(E) Plot of the % fluorescence recovery after photobleaching (FRAP) of Cy5-PC in the SLB before and 30 min after extract addition (mean ± S.E.M., before extract: n = 6 bleach regions from two independent experiments, after extract: n = 9 bleach regions from three independent experiments). Before extract, mobile fraction = 76.85 ± 0.82%, $t_{1/2}$ = 33.21 ± 2.08 s (mean ± SD). After extract addition, the mobile fraction and $t_{1/2}$ could not be calculated due to slow recovery.

See also Video S3.

that SLB fluidity dramatically decreased after extract addition. Taken together with our finding that transferring extract to a fresh SLB supports the formation of a second excitable wave, our data indicate that membrane fluidity plays an important role in the emergence of excitable waves.

We also considered the possibility that there could be limiting components, which are consumed during the first excitable wave, preventing the continued propagation of additional excitable waves. We tested this possibility by supplementing guanosine triphosphate (GTP) (Figure S3A) or increasing the volume of the extract relative to the surface area of the SLBs (Figure S3B). Neither of these adjustments changed the solitary nature of excitable waves. Next, we increased the relative proportion of $PI(4,5)P_2$ (Phosphatidylinositol 4,5-bisphosphate), which is known to regulate active Rho,[14,15] in the SLBs, and we did not observe additional excitable waves or a significant change in oscillatory dynamics (Figure S3C). We also investigated whether the coherent oscillations could develop into propagating excitable waves by extending the phase of the extract cell cycle in which the cortex can support excitability (low Cdk1 activity, I-phase)[16] and preventing the extract from transitioning into M-phase where actomyosin is contractile.[10,11,16,17] Blocking cell cycle progression with RO-3306 (a Cdk1 inhibitor) did not extend the lifetime of oscillations or promote the transition

(E) Morlet power spectra of the active Rho and F-actin dynamics averaged over all boxes constituting the whole field of view shown in (A). Dashed lines indicate dominant oscillatory periods.

(F) Temporal cross correlation between active Rho and F-actin fluorescence signals. Dashed line indicates the time shift of 25 s between the two oscillations.

See also Figure S2 and Video S2.

from oscillatory to excitable dynamics (Figure S3D). Finally, we investigated whether the concentration of the egg extract influenced the propensity to form coherent oscillations. Surprisingly, diluting the extract with buffer did not impair the formation of reconstituted oscillations (Figure S3E), which is in contrast to other extract-based approaches[11,16] and suggests that the coherent oscillations are highly robust and can develop even at low concentrations of the components in *Xenopus* extract.

Reconstituted Rho and F-actin oscillations and waves require Rho activity and polymerized F-actin

Given the quantifiable similarities between the reconstituted Rho oscillations and *in vivo* cortical waves, we next asked whether the molecular mechanism that underlies cortical Rho dynamics was conserved in the reconstituted system. We first investigated whether Rho activity is required for the dynamic Rho and F-actin patterning observed on SLBs. To test this, we treated the extract with a Rho activity inhibitor, C3 transferase, prior to adding the extract to the SLB.[18] Using two concentrations of C3 transferase (33 μg/mL and 100 μg/mL), we found that treatment with C3 prevented both oscillatory and excitable dynamics of Rho and F-actin (Figures 4A and 4B).[19] We also treated extract with 100 μg/mL C3 after oscillations had developed for 15 min and observed a rapid decrease in active Rho and F-actin signal after C3 addition compared to a buffer control (Figure S4A). These data indicate that Rho activity is essential for the observed dynamic patterning in the reconstituted system. This result is in agreement with the work done in *Xenopus* and starfish embryos[7] and suggests that Rho-mediated positive feedback is needed for cortical excitability and oscillations.

We next investigated whether F-actin is required for the emergence of reconstituted cortical dynamics. In starfish embryos, treatment with the actin polymerization inhibitor Latrunculin B resulted in a brief increase in Rho wave amplitude as cortical actin was reduced. This was followed by the disappearance of cortical Rho waves when cortical actin was completely lost, leading to the proposal that F-actin is an essential part of the negative feedback in cortical excitability.[7] We, therefore, allowed oscillations to develop for 30 min before adding a vehicle control (DMSO) or 15 μM Latrunculin B (Figure 4C; Video S4). Control DMSO-treated extract continued to produce dynamic Rho and F-actin oscillations on the SLB, as observed in kymographs of active Rho and F-actin (Figure 4D), whereas in Latrunculin B-treated extract, the F-actin and Rho activity oscillations rapidly disappeared (Figure 4D). We quantified the mean whole field fluorescence intensity of active Rho and F-actin over time and found that in control DMSO-treated extract, the amount of active Rho and F-actin associated with the SLB continued to increase after DMSO addition (Figure 4E). In contrast, the fluorescence signals of active Rho and F-actin rapidly and completely vanished after Latrunculin B addition (Figure 4E), demonstrating that polymerized F-actin is required for the observed spatiotemporal dynamics.

Additionally, we treated extract with varying concentrations of Latrunculin B prior to adding the extract to the SLB (Figure S4B) and saw no change in the temporal period or temporal shift of oscillations, although higher concentrations of Latrunculin B decreased the amplitude of active Rho oscillations (Figures S4C and S4D). We also sought to suppress cortical F-actin bundles with pharmacological inhibitors targeted against specific actin regulatory proteins including formins (SMIFH2) and Rho kinase (H1152). We did not observe a significant difference in the temporal period or temporal shift in extract treated with these drugs compared to control extract (Figures S4E and S4F).

Our real-time addition of Latrunculin B result differs from the effect of Latrunculin B addition in starfish embryos, where F-actin disassembly leads to a transient increase in Rho activity before cortical waves are extinguished.[7] However, in both systems, F-actin disassembly leads to the eventual loss of cortical patterning, suggesting that F-actin is an essential regulator of cortical Rho dynamics. These results, taken together with our finding that Rho activity is required for reconstituted dynamics, demonstrate that the molecular mechanisms underlying reconstituted cortical oscillations and waves recapitulate mechanisms underlying cortical waves in cells.[7]

Conclusions

The experiments presented here provide, to the best of our knowledge, the first reconstitution of oscillatory, Rho GTPase-driven actin dynamics in a cell-free system. The fact that such complex behaviors arise following the combination of cell extract with SLBs directly confirms the ability of the cell cortex to self-organize into complex, dynamic patterns, as originally proposed by E.E. Just more than 80 years ago.[1]

This reconstituted system offers some distinct advantages over cell-based approaches for studying cortical dynamics including the ability to modify the lipid bilayer composition, add recombinant proteins, remove proteins through immunodepletion, and easily add peptide or small molecule inhibitors. Additionally, imaging a two-dimensional cortex is more straightforward than imaging a three-dimensional cell, where the cortex changes shape to accommodate cell movement and cytokinesis.[7–10] This system, however, is not well suited for studies investigating feedback between membrane topologies and cortical waves, as has been characterized in mast cells.[20,21]

The reconstituted cortical Rho waves and oscillations shown here exhibit many properties that are similar to cortical waves described in developing embryos;[7,9] however, there are also clear differences. The excitable, traveling active Rho and F-actin waves identified here do not form a periodic pattern, which our data suggest may be due to changes in SLB fluidity after extract addition. Alternatively, accumulation of bundled F-actin may not provide the right balance of negative feedback to support Rho excitability without suppressing wave propagation.[7–9] Another difference is that reconstituted oscillatory dynamics do not show robust propagation in space. Close inspection of kymographs of oscillations (Figure 2B) suggests there may be short-lived local propagation that is not detectable by our analysis methods. The differences in cortical dynamics between cells and the cell-free system call for further investigation. Identifying the factor(s) that underlie these differences will deepen our understanding of the molecular mechanisms that support self-organization of cortical excitability.

A reconstituted system such as the one presented here could be a powerful approach for studying other types of cortical dynamics including cortical waves that have been identified in migrating cells,[5,6] contractile actomyosin pulses in worm and mouse embryos,[3,4] and subcellular oscillations in non-motile cells.[22] An extract-based reconstituted system also serves as

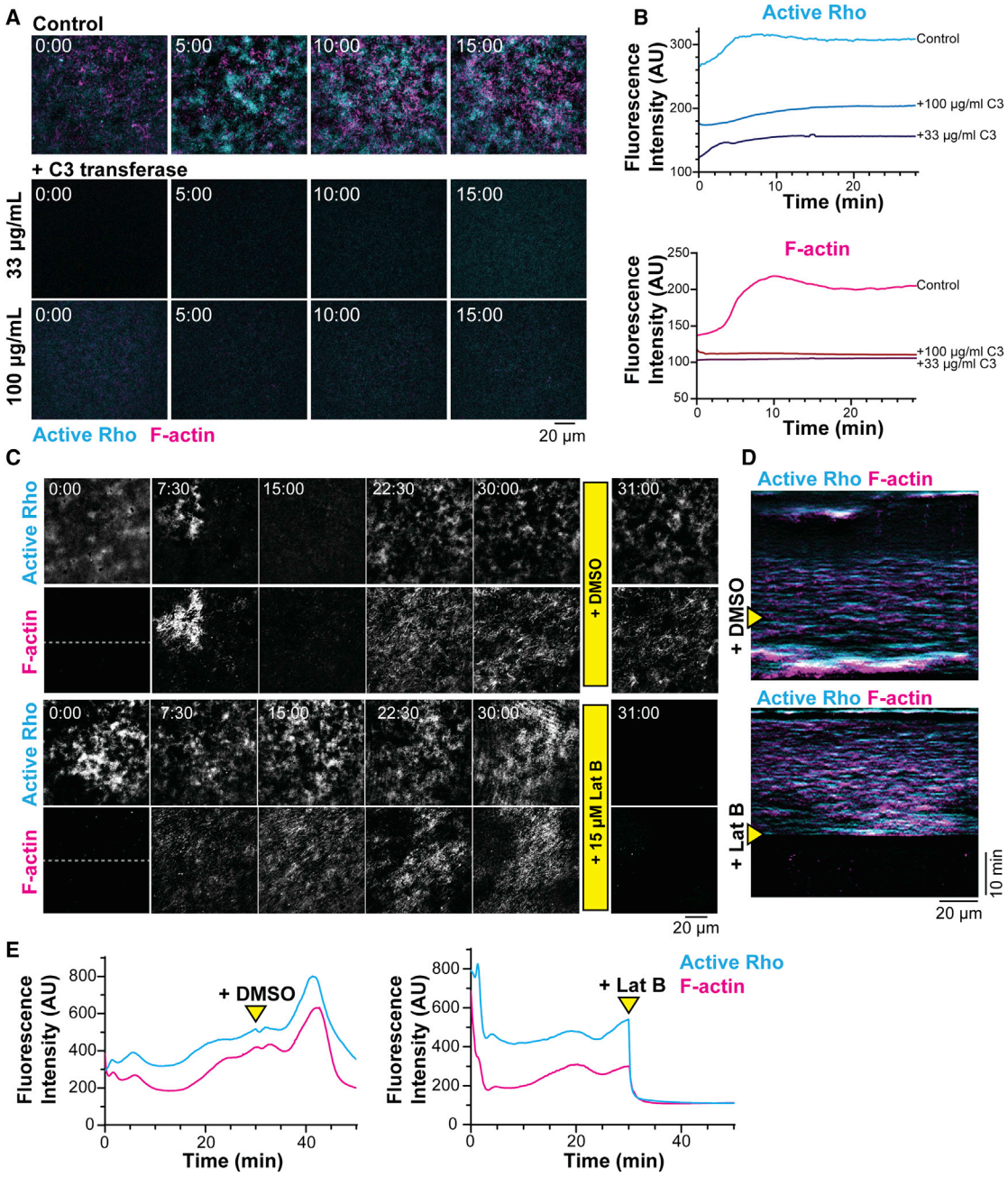

Figure 4. Oscillations in the reconstituted cortex require Rho activity and F-actin polymerization

(A) Active Rho (cyan) and F-actin (magenta) dynamics in a control cortex (top) or following treatment with the Rho inhibitor C3 transferase (33 ug/mL or 100 ug/mL). Time is in minutes:seconds.

(B) Quantification of mean fluorescence intensity of active Rho (cyan) and F-actin (magenta) averaged over the whole field of view in control and C3 transferase-treated extract.

(C) Active Rho and F-actin dynamics before and after addition of DMSO (vehicle control) or 15 µM Latrunculin B. Time is in minutes:seconds. Yellow bars represent the time of DMSO/Latrunculin B addition (30 min). Dashed lines represent regions used to generate kymographs.

(D) Kymographs of active Rho (cyan) and F-actin (magenta) generated from a 10-pixel-wide line, as indicated in (C). Yellow arrowheads represent the time of DMSO or 15 µM Latrunculin B addition.

(E) Mean whole field fluorescence intensity of Active Rho (cyan) and F-actin (magenta) over time in extract treated with DMSO or 15 µM Latrunculin B. Yellow arrowheads indicate time of DMSO or 15 µM Latrunculin B addition.

See also Figures S3 and S4 and Video S4.

a bridge to a fully reconstituted system consisting exclusively of purified components. Recombinant Rho can dynamically and reversibly interact with a SLB,[23,24] suggesting that investigating fully reconstituted excitability using minimal components—just recombinant proteins and a SLB—could be possible in the future. Overall, cell-free reconstitution of cortical Rho dynamics is an important step toward dissecting the molecular mechanisms of cellular morphogenesis and biological pattern formation and is broadly applicable to a variety of essential cellular functions.

STAR★METHODS

Detailed methods are provided in the online version of this paper and include the following:

- KEY RESOURCES TABLE
- RESOURCE AVAILABILITY
  - Lead contact
  - Materials availability
  - Data and code availability
- EXPERIMENTAL MODEL AND SUBJECT DETAILS
- METHOD DETAILS
  - Preparation of supported lipid bilayers
  - Preparation of imaging chambers
  - Preparation of F-actin intact M-phase *Xenopus* egg extract
  - Converting to interphase extract and monitoring the cell cycle state
  - Preparation of reactions for live imaging
  - Generation of new DNA constructs
  - Expression and purification of recombinant protein
  - Live imaging
  - Drug treatments and perturbations
- QUANTIFICATION AND STATISTICAL ANALYSIS
  - Figure preparation
  - Analysis of oscillatory dynamics
  - Analysis of excitable waves
  - Whole field intensity measurements
  - FRAP analysis

SUPPLEMENTAL INFORMATION

Supplemental information can be found online at https://doi.org/10.1016/j.cub.2021.10.021.

ACKNOWLEDGMENTS

We would like to thank the members of the Miller, Bement, Goryachev, and Vecchiarelli labs for their feedback on this research and comments on the manuscript. We thank George von Dassow for his contributions to our thinking about cortical excitability and Kevin Sonnemann and Thomas Burke for their assistance in reagent generation. This work was funded by NSF grants 1615338 (A.L.M.), 1614190 (W.M.B.), and BBSRC grants BB/P006507 and BB/P01190X (A.B.G.). A.G.V. is supported by NSF 1817478. C.M.F. is supported by NIH R35GM131753. J.L. is supported by an American Cancer Society Postdoctoral Fellowship.

AUTHOR CONTRIBUTIONS

Conceptualization, J.L. and A.L.M.; methodology, J.L., C.M.F., A.G.V., and A.L.M.; software, M.L. and A.B.G.; validation, J.L. and M.L.; formal analysis, J.L. and M.L.; investigation, J.L.; resources, A.L.M., A.G.V., and M.P.; writing—original draft, J.L., M.L., K.S., A.B.G., and A.L.M.; writing—review & editing, all authors; visualization, J.L. and M.L.; supervision, W.M.B., A.B.G., and A.L.M; project administration, A.B.G. and A.L.M.; funding acquisition, W.M.B., A.B.G., and A.L.M.

DECLARATION OF INTERESTS

The authors declare no competing interests.

Received: April 13, 2021
Revised: September 7, 2021
Accepted: October 8, 2021
Published: November 4, 2021

REFERENCES

1. Just, E.E. (1939). The Biology of the Cell Surface (P. Blakiston's Son & Co.).
2. Green, R.A., Paluch, E., and Oegema, K. (2012). Cytokinesis in animal cells. Annu. Rev. Cell Dev. Biol. *28*, 29–58.
3. Michaux, J.B., Robin, F.B., McFadden, W.M., and Munro, E.M. (2018). Excitable RhoA dynamics drive pulsed contractions in the early *C. elegans* embryo. J. Cell Biol. *217*, 4230–4252. https://doi.org/10.1083/jcb.201806161.
4. Maître, J.L., Niwayama, R., Turlier, H., Nédélec, F., and Hiiragi, T. (2015). Pulsatile cell-autonomous contractility drives compaction in the mouse embryo. Nat. Cell Biol. *17*, 849–855. https://doi.org/10.1038/ncb3185.
5. Weiner, O.D., Marganski, W.A., Wu, L.F., Altschuler, S.J., and Kirschner, M.W. (2007). An actin-based wave generator organizes cell motility. PLoS Biol. *5*, e221. https://doi.org/10.1371/journal.pbio.0050221.
6. Iglesias, P.A., and Devreotes, P.N. (2012). Biased excitable networks: how cells direct motion in response to gradients. Curr. Opin. Cell Biol. *24*, 245–253. https://doi.org/10.1016/j.ceb.2011.11.009.
7. Bement, W.M., Leda, M., Moe, A.M., Kita, A.M., Larson, M.E., Golding, A.E., Pfeuti, C., Su, K.C., Miller, A.L., Goryachev, A.B., and von Dassow, G. (2015). Activator-inhibitor coupling between Rho signalling and actin assembly makes the cell cortex an excitable medium. Nat. Cell Biol. *17*, 1471–1483. https://doi.org/10.1038/ncb3251.
8. Goryachev, A.B., Leda, M., Miller, A.L., von Dassow, G., and Bement, W.M. (2016). How to make a static cytokinetic furrow out of traveling excitable waves. Small GTPases *7*, 65–70. https://doi.org/10.1080/21541248.2016.1168505.
9. Michaud, A., Swider, Z.T., Landino, J., Leda, M., Miller, A.L., von Dassow, G., Goryachev, A.B., and Bement, W.M. (2021). Cortical excitability and cell division. Curr. Biol. *31*, R553–R559. https://doi.org/10.1016/j.cub.2021.02.053.
10. Nguyen, P.A., Groen, A.C., Loose, M., Ishihara, K., Wühr, M., Field, C.M., and Mitchison, T.J. (2014). Spatial organization of cytokinesis signaling reconstituted in a cell-free system. Science *346*, 244–247. https://doi.org/10.1126/science.1256773.
11. Field, C.M., Pelletier, J.F., and Mitchison, T.J. (2017). Xenopus extract approaches to studying microtubule organization and signaling in cytokinesis. Methods Cell Biol. *137*, 395–435. https://doi.org/10.1016/bs.mcb.2016.04.014.
12. Benink, H.A., and Bement, W.M. (2005). Concentric zones of active RhoA and Cdc42 around single cell wounds. J. Cell Biol. *168*, 429–439.
13. Taniguchi, D., Ishihara, S., Oonuki, T., Honda-Kitahara, M., Kaneko, K., and Sawai, S. (2013). Phase geometries of two-dimensional excitable waves govern self-organized morphodynamics of amoeboid cells. Proc. Natl. Acad. Sci. USA *110*, 5016–5021. https://doi.org/10.1073/pnas.1218025110.
14. Yoshida, S., Bartolini, S., and Pellman, D. (2009). Mechanisms for concentrating Rho1 during cytokinesis. Genes Dev. *23*, 810–823. https://doi.org/10.1101/gad.1785209.

15. Budnar, S., Husain, K.B., Gomez, G.A., Naghibosadat, M., Varma, A., Verma, S., Hamilton, N.A., Morris, R.G., and Yap, A.S. (2019). Anillin Promotes Cell Contractility by Cyclic Resetting of RhoA Residence Kinetics. Dev. Cell *49*, 894–906. https://doi.org/10.1016/j.devcel.2019.04.031.

16. Field, C.M., Nguyen, P.A., Ishihara, K., Groen, A.C., and Mitchison, T.J. (2014). Xenopus egg cytoplasm with intact actin. Methods Enzymol. *540*, 399–415. https://doi.org/10.1016/B978-0-12-397924-7.00022-4.

17. Canman, J.C., Hoffman, D.B., and Salmon, E.D. (2000). The role of pre- and post-anaphase microtubules in the cytokinesis phase of the cell cycle. Curr. Biol. *10*, 611–614.

18. Huelsenbeck, J., Dreger, S.C., Gerhard, R., Fritz, G., Just, I., and Genth, H. (2007). Upregulation of the immediate early gene product RhoB by exoenzyme C3 from Clostridium limosum and toxin B from Clostridium difficile. Biochemistry *46*, 4923–4931. https://doi.org/10.1021/bi602465z.

19. Just, I., Richter, H.P., Prepens, U., von Eichel-Streiber, C., and Aktories, K. (1994). Probing the action of Clostridium difficile toxin B in Xenopus laevis oocytes. J. Cell Sci. *107*, 1653–1659.

20. Wu, Z., Su, M., Tong, C., Wu, M., and Liu, J. (2018). Membrane shape-mediated wave propagation of cortical protein dynamics. Nat. Commun. *9*, 136. https://doi.org/10.1038/s41467-017-02469-1.

21. Wu, M., and Liu, J. (2021). Mechanobiology in cortical waves and oscillations. Curr. Opin. Cell Biol. *68*, 45–54. https://doi.org/10.1016/j.ceb.2020.08.017.

22. Wu, M., Wu, X., and De Camilli, P. (2013). Calcium oscillations-coupled conversion of actin travelling waves to standing oscillations. Proc. Natl. Acad. Sci. USA *110*, 1339–1344. https://doi.org/10.1073/pnas.1221538110.

23. Golding, A.E., Visco, I., Bieling, P., and Bement, W.M. (2019). Extraction of active RhoGTPases by RhoGDI regulates spatiotemporal patterning of RhoGTPases. eLife *8*, e50471. https://doi.org/10.7554/eLife.50471.

24. Graessl, M., Koch, J., Calderon, A., Kamps, D., Banerjee, S., Mazel, T., Schulze, N., Jungkurth, J.K., Patwardhan, R., Solouk, D., et al. (2017). An excitable Rho GTPase signaling network generates dynamic subcellular contraction patterns. J. Cell Biol. *216*, 4271–4285. https://doi.org/10.1083/jcb.201706052.

25. Schindelin, J., Arganda-Carreras, I., Frise, E., Kaynig, V., Longair, M., Pietzsch, T., Preibisch, S., Rueden, C., Saalfeld, S., Schmid, B., et al. (2012). Fiji: an open-source platform for biological-image analysis. Nat. Methods *9*, 676–682. https://doi.org/10.1038/nmeth.2019.

26. Murray, A.W., and Kirschner, M.W. (1989). Cyclin synthesis drives the early embryonic cell cycle. Nature *339*, 275–280. https://doi.org/10.1038/339275a0.

STAR★METHODS

KEY RESOURCES TABLE

REAGENT or RESOURCE	SOURCE	IDENTIFIER
Chemicals, peptides, and recombinant proteins		
Latrunculin B	Tocris Bioscience	Cat # 3974
C3 transferase	Cytoskeleton	Cat # CT03
RO-3306	Santa Cruz Biotechnology	Cat # sc-358700A
GTP	ThermoFisher	Cat # 18332015
SMIFH2	Sigma	Cat # S4826
H1152	Cayman Chemical	Cat # 10007653
Brain PS	Avanti	Cat # 840032P
Brain PC	Avanti	Cat # 840053P
Cy5 PC	Avanti	Cat # 850483
Liver PI	Avanti	Cat # 840042P
Brain PI(4,5)P_2	Avanti	Cat # 840046X
FLAG-GFP-rGBD	[7]	N/A
FLAG-Cys-UtrCH	This study	N/A
Alexa Fluor™ 647 C_2 Maleimide Labeling Kit	ThermoFisher	Cat # A20347
Alexa Fluor™ 594 C_2 Maleimide Labeling Kit	ThermoFisher	Cat # A10239
Experimental models: organisms/strains		
Oocyte Positive Female *Xenopus laevis*, Pigmented	Nasco	Cat # LM00531
Oligonucleotides		
Primer for creating pFastBac1/FLAG-Cys-UtrCH: ATAGCGGCCGCACCATGGACTACAAGGACGACG ATGACAAGGGTTGTGGAATGGCCAAGTATGGAG	IDT	N/A
Primer for creating pFastBac1/FLAG-Cys-UtrCH: TGAGCTCGAGTTAGTCTATGGTGAC	IDT	N/A
Recombinant DNA		
pFastBac1/FLAG-GFP-rGBD	[7]	N/A
pFastBac1/FLAG-Cys-UtrCH	This study	N/A
pFastBac1	ThermoFisher	Cat # 10359016
Software and algorithms		
Fiji	Open Source[25]	https://imagej.net/software/fiji/
Microsoft Excel for Windows	Microsoft	https://www.microsoft.com/en-us/
Prism	Graphpad	https://www.graphpad.com/
MATLAB 2020a	MathWorks	https://www.mathworks.com/products/matlab.html
Custom code for analyzing waves and oscillations	This study	https://doi.org/10.5281/zenodo.5532754
Other		
Custom Metal Coverglass Mounts	University of Michigan Scientific Instrument Shop	N/A
Coverglass 22 mm No.1.5	ThermoFisher	Cat # 12-542-B
Edmund Optics Norland Optical Adhesive No. 61	ThermoFisher	Cat # NC9468157
Flat cap 0.2 mL PCR tubes	Sigma	Cat # CLS6571-960EA
Thin-walled Ultra-clear tubes 11 × 60 mm	Beckman	Cat # 344062
Anti-FLAG M2 Affinity Gel	Sigma	Cat # A2220

RESOURCE AVAILABILITY

Lead contact

Further information and requests for resources and reagents should be directed to and will be fulfilled by the Lead Contact, Ann L. Miller (annlm@umich.edu)

Materials availability

Plasmids generated in this study can be obtained from co-author William Bement (wmbement@wisc.edu)

Data and code availability

- Microscopy data reported in this paper will be shared by the lead contact upon request.
- Custom code used in this study has been deposited on Zenodo and is publicly available as of the date of publication. The DOI is listed in the Key Resources Table.
- Any additional information required to reanalyze the data reported in this paper is available from the lead contact upon request.

EXPERIMENTAL MODEL AND SUBJECT DETAILS

Adult *Xenopus laevis* wild type female frogs were purchased from Nasco or *Xenopus* 1. Female frogs were injected with human chorionic gonadotropin (HCG) to induce them to lay eggs.

Frogs were housed in a recirculating tank system (Tecniplast), which constantly monitors water quality parameters (temperature, pH, and conductivity) to ensure safe and consistent water quality for an optimal environment for frog health. Daily health and maintenance checks were performed by Animal Care Staff, and frogs were fed frog brittle (Nasco) two times per week.

All studies strictly adhered to the compliance standards of the US Department of Health and Human Services Guide for the Care and Use of Laboratory Animals and were approved by the University of Michigan's Institutional Animal Care and Use Committee. A board-certified Laboratory Animal Veterinarian oversees our animal facility.

METHOD DETAILS

Preparation of supported lipid bilayers

Powder lipid stocks (Avanti Polar Lipids, see Key Resources Table) were resuspended to working concentrations in chloroform ($CHCl_3$, Sigma). Chloroform-suspended lipids were combined in the following molar ratios: 0.6 PC, 0.3 PS, 0.1 PI (stock A), or 0.6 PC, 0.3 PS, 0.05 PI, and 0.05 PI(4,5)P_2 (stock B), or 0.5 PC, 0.1 Cy5 PC 0.3 PS, 0.1 PI (stock C). Lipid stocks were dried using N_2 gas and kept warm on a 42°C heat block.[11] Dried lipid stocks were vacuum dessicated for 1 h at 45°C using a centrifugal vacuum (CentriVap, ThermoFisher Scientific). Under N_2 atmosphere, lipid stocks were resuspended to a final concentration of 5 mM using high-salt extract buffer (HS-XB 200 mM KCl, 1 mM $MgCl_2$, 0.1 mM $CaCl_2$), vortexed, incubated at 37°C for 30 min, and vortexed again. Lipid stocks were then sonicated to generate small unilamellar vesicles (SUVs) using a cup horn sonicator system (700 Watt Sonicator system 110V, QSONICA) in polystyrene tubes at 80W for 10 min with pulsed sonication (30 s on, 10 s off) at room temperature with N_2 atmosphere. SUVs were sterile filtered using a 0.22 μm filter (Millipore) under N_2 atmosphere into borosilicate glass vials (ThermoFisher Scientific) and stored at −20°C for less than 3 months.

To prepare supported lipid bilayers (SLBs), SUVs were thawed at room temperature under N_2 atmosphere. Lipid stocks A and B were mixed at the appropriate ratios to generate 0.1%, 2%, and 5% PI(4,5)P_2 solutions.[11] To prepare labeled SLBs, labeled stock C was added to a 0.1% PI(4,5)P_2 solution at a 1.25 x10^{-4} molar ratio. Lipid solutions were sonicated for 5 min as described above at room temperature and under N_2 atmosphere. The sonicated SUVs were diluted to 0.5 mM using HS-XB, and $CaCl_2$ was added to a 4 mM final concentration. SUVs were added to O_2 plasma-cleaned chambers (approximately 30 μL per chamber). SLBs were incubated at 42°C for 30 min, and washed three times with three volumes of extract buffer (XB: 100 mM KCl, 1 mM $MgCl_2$, 10 mM HEPES, pH 7.7), taking care to maintain a layer of liquid above the SLB.[11] Washed wells were kept at room temp for less than 4 h before adding extract.

Preparation of imaging chambers

Coverglasses (24 × 50 mm No. 1.5, VWR) were washed in a solution of 2% Hellmanex III (Sigma) for 2 h at 70°C with constant stirring. Coverglasses were rinsed thoroughly with deionized water and allowed to dry overnight in a dust-free chamber until assembly of imaging chambers. A cleaned coverglass was attached to a custom aluminum coverglass mount, comprised of a rectangular slide with a central oval-shaped opening and clamps on either end to hold the coverglass in place (University of Michigan, Scientific Instrument Shop). The cap and lower third of 0.2 mL PCR tubes (Sigma) were removed to create wells for imaging extract.[11] The rim of the PCR tube was dotted with UV glue (Norland Optical Adhesive No. 61, ThermoFisher Scientific) and adhered to the coverglass using 365 nM UV light for one minute. Additional glue was used to reinforce the attachment of the wells, and chambers were exposed to 365 nM UV light for 30 min. Chambers were stored in a dust-free container at room temperature until use.

Immediately prior to adding SUVs, imaging chambers were O_2 plasma cleaned (PE25-JW Benchtop Plasma Cleaning System, PLASMA ETCH) for 10 min.

Preparation of F-actin intact M-phase *Xenopus* egg extract

Adult, female *Xenopus laevis* were induced to lay eggs using HCG in Ca^{2+}-free Marc's Modified Ringers (Ca^{2+}-free MMR: 100 mM NaCl, 2 mM KCl, 1 mM $MgCl_2$, 100 μM EGTA, 5 mM HEPES, pH 7.8).[26] Eggs were de-jellied in 2% cysteine (Sigma) in Ca^{2+}-free MMR, pH 7.8 and rinsed in three volumes of cytostatic factor extract buffer (CSF-XB: XB + 1 μM $MgCl_2$, 5 mM EGTA). Lysed or activated eggs were removed as needed. Eggs were washed with CSF-XB plus protease inhibitors (LPC: 10 μg/mL leupeptin, pepstatin A, and chymostatin, all from Sigma) and transferred to a thin-walled UltraClear centrifuge tube (Beckman Coulter). Eggs were packed using a clinical centrifuge at 700 x g for 30 s and then 1,400 x g for 15 s.[11] Remaining buffer was aspirated using a vacuum, and packed eggs were kept on ice. To crush, centrifuge tubes were transferred to a swinging bucket rotor (TH-660, ThermoFisher Scientific) and centrifuged (Sorvall WX+ Ultracentrifuge, ThermoFisher Scientific) at 15,000 x g for 15 min at 4°C. Cytoplasmic extract was harvested by punching through the side of the tube using an 18G needle and 1 mL syringe and deposited in a 1.5 mL tube on ice.[11] Protease inhibitors (LPC) were added to a final concentration of 10 μg/mL along with energy mix to a final concentration of 9 mM (energy mix: creatine phosphate, 1 mM ATP, 1 mM $MgCl_2$, all from Sigma).[11] This extract is arrested in metaphase of meiosis II.[16]

Converting to interphase extract and monitoring the cell cycle state

A controlled release of M-phase arrested extract into interphase (I-phase) is desired. A gelation-contraction assay was used to evaluate the cell cycle state of the isolated extract. Several 2 μL droplets of extract were pipetted under heavy mineral oil (ThermoFisher Scientific) in a Petri dish, and light scattering was monitored using a stereoscope. Extract was generally considered high quality if droplets from the (M-phase) control aliquot showed contraction to the droplet center after 5 min.[16] If the extract does not contract, the M-phase arrest was released during the extract preparation, and therefore, the extract was not used. To convert the extract to interphase (I-phase), $CaCl_2$ was added to a single 200 μL aliquot of extract to a final concentration of 0.4 mM, with vigorous mixing.[11,16] Extract was incubated for 5 min at room temperature before assessing cell cycle state. Using the gelation-contraction assay, the extract was deemed to be in I-phase if the light scattering particles did not contract toward the center of the droplet after 5 min.[11]

Preparation of reactions for live imaging

After I-phase cell cycle state was confirmed, extract was placed on ice while reactions were prepared. Recombinant fluorescent protein probes, GFP-rGBD and UtrCH-647 were diluted to working concentrations in freshly-cycled I-phase extract. GFP-rGBD was added to the reaction mixture at a final concentration of 750 nM, and UtrCH-647 was added at a final concentration of 100 nM. For co-imaging with Cy5 PC, UtrCH-594 was added at a final concentration of 100 nM. After washing with XB, SLBs were washed three times with 30 μL freshly cycled I-phase extract, taking care not to expose the SLBs to air. To investigate excess extract volume, reactions were prepared using 90 μL (instead of 30 μL) I-phase extract with 750 nM GFP-rGBD and 100 nM UtrCH-647. For extract dilution experiments, I-phase extract was diluted 20, 40, or 60% using 1X XB before adding GFP-rGBD and UtrCH-647 to 750 nM and 100 nM, respectively. The reaction mixture was added to the SLB, and the chamber was immediately taken to the microscope for live imaging. For SLB transfer experiments, after an excitable was imaged, the full 30 μL of the extract reaction containing 750 nM GFP-rGBD and 100 nM UtrCH-647 was pipette-transferred from one well to a new well that was freshly washed with I-phase extract prior to addition of the transferred reaction. Working stocks of GFP-rGBD, UtrCH-594, and UtrCH-647 diluted in I-phase extract were aliquoted, frozen in liquid N_2, and stored at −80°C.

Generation of new DNA constructs

Primers for pFastBac1/FLAG-Cys-UtrCH are listed in the key resources table. The described construct was engineered by PCR so that the amino acid sequence immediately N-terminal to the Utrophin start site is: M*DYKDDDDK*G**C**G, where *FLAG-tag* is in italics and the lone **cysteine** residue is in bold. The resultant amplicon was cloned into the bacmid donor plasmid pFastBac1 (ThermoFisher). The described construct was verified by sequencing.

Expression and purification of recombinant protein

For recombinant protein expression, pFastBac1 clones encoding FLAG-Cys-UtrCH and FLAG-GFP-rGBD[7] were used to generate recombinant bacmids in DH10BAC (Invitrogen) bacteria. Sf21 insect cells were transfected with the recombinant bacmids, and subsequent recombinant baculoviruses were used to infect additional Sf21 monolayers. Recombinant proteins were purified using anti-FLAG M2 affinity resin (Sigma) with Arg-based elution.[7] Elution fractions were pooled and the protein concentrated in 25 mM HEPES, 100 mM KCl pH 7.5 prior to labeling. For labeling, Alexa Fluor 647 C_2 maleimide or Alexa Fluor 594 C_2 maleimide was conjugated to the purified UtrophinCH protein via the lone cysteine residue according to the label manufacturer's instructions (ThermoFisher).

Live imaging

TIRF microscopy was performed using a Nikon Ti2-E motorized inverted microscope with perfect focus, motorized TIRF module, and a LUN-F laser light source (488nm (90mW), 561nm (70mW), and 640nm (65mW)) all controlled by NIS Elements software. A TIRF Quad Dichroic cube (C-FL TIRF Ultra Hi S/N 405/488/561/638 Quad Cube, Z Quad HC Cleanup, HC TIRF Quad Dichroic, in metal

cube, HC Quad Barrier Filter) was used with a 60X Objective lens (CFI60 Apochromat TIRF 60X Oil Immersion Objective Lens N.A. 1.49, W.D. 0.12 mm, F.O.V 22 mm) and a Photometrics Prime 95B Back-illuminated sCMOS camera.

Generally, live imaging began within three minutes of completing the buffer and extract washes and adding extract plus recombinant proteins to the SLB. Extract was imaged in the appropriate channel at 5 or 10 s intervals for 60-90 min. Perfect focus was used for the duration of the imaging session.

For FRAP experiments, a 20 μm x 20 μm box was bleached with a 405 nM laser for 100 ms at 5% laser power. The SLB was imaged for 10 s prior to bleaching and for 5 min after bleaching. Three independent bleach regions were tested in three fields of view. The same SLB was bleached prior to extract addition and 30 min after extract addition, only in reactions where cortical oscillations were present. Cy5 PC was also co-imaged during the reaction.

Drug treatments and perturbations

Lyophilized C3 transferase (Cytoskeleton) was resuspended in buffer containing: 500 mM imidazole, 50 mM TrisHCl, pH 7.5, 10 mM $MgCl_2$, 200 mM NaCl, 5% sucrose, 1% dextran and supplemented with 1 mM DTT. C3 transferase was aliquoted, frozen in liquid N_2, and stored at −80°C until use. Where indicated, C3 transferase or a buffer control (1X XB) was added to the extract at a final concentration of 100 μg/mL or 33 μg/mL immediately before extract was added to the SLBs. For real-time addition of C3 transferase, an equivalent volume of I-phase extract containing 2X C3 transferase (final concentration of 100 μg/mL) or buffer (1X XB) was added to the imaging chamber at the time indicated. Extract containing 2X C3 transferase or buffer was kept at room temperature before adding to the imaging chamber.

For GTP addition, GTP (ThermoFisher) was added to the extract at a final concentration of 1 mM immediately before adding the reaction to the SLB.

For RO-3306 treatment, RO-3306 (Santa Cruz Biotechnology) was resuspended in DMSO to a working concentration of 1 mM, aliquoted and stored at −20°C. RO-3306 was added to the extract at a final concentration of 50 μM or 100 μM immediately before extract was added to the SLBs.

Latrunculin B powder (Tocris Bioscience) was resuspended in DMSO (Sigma) to a working concentration of 1 mM and stored at −20°C. Latrunculin B, or an equivalent volume of DMSO, was added to the extract at 100nM, 1 μM, or 10 μM prior to adding the extract to the SLB. For real-time addition of Latrunculin B, an equivalent volume of I-phase extract containing 2X Latrunculin B (final concentration of 15 μM) or DMSO was added to the imaging chamber at the time indicated. Extract containing 2X Latrunculin B or DMSO was kept at room temperature before adding to the imaging chamber.

SMIFH2 (Sigma) was resuspended in DMSO to a working concentration of 10 mM aliquoted and stored at −20°C. SMIFH2 was added to extract reaction at a final concentration of 100 μM before adding the reaction to the SLB.

H1152 (Cayman Chemical) was resuspended in DMSO to a working concentration of 10 mM, aliquoted and stored at −20°C. H-1152 was added to the extract reaction at a final concentration of 400 μM before adding the reaction to the SLB.

QUANTIFICATION AND STATISTICAL ANALYSIS

Figure preparation

Images were processed in Fiji. TIRF images were cropped to the central portion (approximately one-third of the whole field of view, 674x586 pixels for oscillatory and excitable wave videos). Channels were independently adjusted to highlight relevant features, and pseudo-colored as indicated in the figure. Difference subtraction was performed by duplicating time series stacks with a 30 s time difference (e.g., separated by 6 frames at 5 s interval) and using the "Image Subtraction" tool in Fiji. Kymographs were generated using the Multi Kymograph analysis tool in in Fiji. A 10 pixel wide line was drawn horizontally across the middle of the cropped field of view (or where otherwise indicated in the figures) of a difference subtracted video. Kymographs were generated for individual channels and later merged. Fiji's region of interest (ROI) manager was used to ensure fidelity in the placement of the line used to generate kymographs. Kymographs were enlarged 2-fold or 4-fold along the y axis in Fiji with bilinear interpolation to better highlight separation between active Rho and F-actin signal during oscillations and waves.

Analysis of oscillatory dynamics

To avoid optical blur, centrally-located, well-focused subareas of the total field of view (typically 600x600 pixels) were selected for the detailed analysis. Then, the difference subtraction transformation with a delay of n = 6 frames was applied to each image frame as described above (Figure S1A, subpanel 1). Negative values were adjusted to 0. Using analysis of simulated wave patterns, we ensured that such transformation does not change either signal periods or the shift between the signals. Then, the field of view was divided into square boxes of 20x20 pixels, and active Rho and F-actin signals were spatially averaged within the boxes (Figure S1A, subpanel 2). The size of the box was optimized to provide effective reduction of image noise, yet be sufficiently smaller than the characteristic size of the analyzed patterns. This procedure typically resulted in a matrix of 30x30 boxes per field of view. Next, moving normalization was applied to both active Rho and F-actin signals to remove trends. Every frame was normalized by the maximal and minimal values inside a moving window of 40 frames. Following this initial data preparation, Morlet power spectra (using MATLAB function *cwtft('wavelet','morl')*), autocorrelation, and cross-correlation of active Rho and F-actin signals were computed for each box as described elsewhere.[7] Histograms and cumulative statistics were computed over all boxes. Average periods and their standard deviations were computed from the maxima of Morlet spectra as follows. Morlet spectrum maxima were

computed with MATLAB function *findpeaks* for each spatial averaging box and video frame and then averaged over all time points and boxes.

To compute the amplitude of oscillations, unprocessed imaging data were used. Within a given experiment, the amplitude values were first computed in the 20x20 pixel boxes and then averaged over all boxes for the duration of experiment. To remove trends, oscillation amplitude within a single box was computed as the difference between the maximum and the minimum in a moving time window with a duration of 300 s.

Analysis of excitable waves

First, the immobile fraction of signals was removed by the Fourier transform filter as follows. Temporal Fourier transform was computed (using MATLAB function *fft*) for every pixel of the video. Then, pixels corresponding to low frequencies were filtered out, and the inverse fast Fourier transform (using MATLAB function *ifft*) was applied. Following this procedure, the field of view was divided into boxes as described above. The shift between the two signals was computed by averaging the cross-correlation function over the boxes that show the shift between 5 and 50 s. Velocities of waves were determined using kymographs computed on median vertical, median horizontal, and two diagonal lines of the field of view. Each line of the kymograph was subdivided into 20 pixel segments and the amplitude of the signal averaged over each segment. For each segment, the maximum value along the time dimension of kymograph was found using MATLAB function *findpeaks*, and the velocity of the wave was computed from the dynamics of thus identified maxima.

The full width at half-maxima of excitable waves was determined using the same set of kymographs as above. Each horizontal line of the kymograph corresponding to a given time point was analyzed separately. Half widths of waves were found using *findpeaks*, and these results were then averaged over all peaks for the given kymograph line, followed by averaging over time and, finally, across all kymographs.

Whole field intensity measurements

Whole field intensity was measured using difference subtracted images cropped to the central portion of the field of view (674x586 pixels for oscillatory waves, 734x644 pixels for C3 treatment videos and 636x636 pixels for Latrunculin B videos). Minimum, Mean, or Maximum gray value was measured over time using the ''Measure Stack'' tool in Fiji. Intensity versus time was plotted using Microsoft excel or GraphPad Prism.

FRAP analysis

A ROI corresponding to the size of the bleach region (20 μm x 20 μm) was measured for the mean fluorescence intensity over time. A second ROI of the same size, located outside of the bleached region, was used as reference for the change in mean fluorescence intensity over time. Measurements were background corrected using the following equation:

$$I_{norm}(t) = I_{frap}(t) - \Delta I_{ref}(t)$$

Where I_{frap} is the ROI tracking the bleached area, I_{ref} is the ROI tracking a region of the SLB outside the bleached area. Then values were normalized to a percent recovery using the following equation.

$$\%\ recovery(t) = \frac{I_{norm}(t) - I_{bleach}(t)}{I_{prebleach}} \times 100$$

Where I_{bleach} is the intensity immediately after bleaching and $I_{pre\ bleach}$ is the average intensity of the ROI before bleaching. The average % recovery ± SEM was plotted using GraphPad Prism.

The mean % recovery of the ''before extract'' data was fit to a single exponeital associaton curve using the ''analyze'' function in GraphPad Prism. The curve was constrained so that the plateau was £ 100 and the Y0 was set to equal 0. All data points outside of this range were excluded from analysis. The SEM was caclulated using equal variance.